The Cell Surface 2 (2018) 24–37

Contents lists available at ScienceDirect

The Cell Surface

journal homepage: www.journals.elsevier.com/the-cell-surface

Nascent teichoic acids insertion into the cell wall directs the localization and activity of the major pneumococcal autolysin LytA

J. Bonnet[a], C. Durmort[a], I. Mortier-Barrière[b], N. Campo[b], M. Jacq[a,1], C. Moriscot[a], D. Straume[c], K.H. Berg[c], L. Håvarstein[c], Y.-S. Wong[d], T. Vernet[a], A.M. Di Guilmi[a,*,2]

[a] Institut de Biologie Structurale (IBS), Univ. Grenoble Alpes, CEA, CNRS, 38044 Grenoble, France
[b] Laboratoire de Microbiologie et Génétique Moléculaires, Centre de Biologie Intégrative (CBI), Centre National de la Recherche Scientifique (CNRS), Université de Toulouse, UPS, F-31000 Toulouse, France
[c] Faculty of Chemistry, Biotechnology and Food Science, Norwegian University of Life Sciences, P.O. Box 5003, NO-1432 Aas, Norway
[d] Département de Pharmacochimie Moléculaire (DPM), Univ. Grenoble Alpes, UMR 5063 CNRS, ICMG FR 2607, 38 041 Grenoble, France

ARTICLE INFO

Keywords:
Streptococcus pneumoniae cell wall
Peptidoglycan hydrolases
Choline-Binding Proteins
Major autolysin LytA localization
Teichoic acids localization

ABSTRACT

The bacterial cell wall is in part composed of the peptidoglycan (PG) layer that maintains the cell shape and sustains the basic cellular processes of growth and division. The cell wall of Gram-positive bacteria also carries teichoic acids (TAs). In this work, we investigated how TAs contribute to the structuration of the PG network through the modulation of PG hydrolytic enzymes in the context of the Gram-positive *Streptococcus pneumoniae* bacterium. Pneumococcal TAs are decorated by phosphorylcholine residues which serve as anchors for the Choline-Binding Proteins, some of them acting as PG hydrolases, like the major autolysin LytA. Their binding is non covalent and reversible, a property that allows easy manipulation of the system.

In this work, we show that the release of LytA occurs independently from its amidase activity. Furthermore, LytA fused to GFP was expressed in pneumococcal cells and showed different localization patterns according to the growth phase. Importantly, we demonstrate that TAs modulate the enzymatic activity of LytA since a low level of TAs present at the cell surface triggers LytA sensitivity in growing pneumococcal cells. We previously developed a method to label nascent TAs in live cells revealing that the insertion of TAs into the cell wall occurs at the mid-cell. In conclusion, we demonstrate that nascent TAs inserted in the cell wall at the division site are the specific receptors of LytA, tuning in this way the positioning of LytA at the appropriate place at the cell surface.

Introduction

The bacterial cell wall maintains the cell shape and sustains the basic cellular processes of growth and division. It is also required to resist turgor pressure and provides an interface between the cell and its environment. Because the cell wall is essential for viability and is composed by molecules not present in eukaryotic host cells, its biosynthetic enzymes have been exploited as successful targets for antibiotic development. The bacterial cell wall is composed of peptidoglycan (PG), a matrix of linear glycan chains of *N*-acetylmuramic acid (Mur*N*Ac) and *N*-acetylglucosamine (Glu*N*Ac) residues, which are cross-linked via peptides composed of l- and d-amino acids. Assembly of the PG network requires synthetic and hydrolytic enzymes. Penicillin-Binding Proteins (PBPs) polymerize the glycan chains (glycosyltransferase activity) and cross-link the stem peptides (transpeptidation activity that is inhibited by β-lactam antibiotics) (for reviews see: Sauvage and Terrak, 2016; Egan et al., 2015). Glycan chains polymerization and peptides cross-link can also be performed by enzymes other than PBPs, like RodA from *Bacillus subtilis*, and l,d-transpeptidases, respectively (Emami et al., 2017; Hugonnet et al., 2016). Endogenous PG hydrolases are divided into different classes according to their substrate specificity and cleave the PG polymer in order to insert new material and to allow daughter cells separation and PG maturation (for review see: Vollmer et al., 2008).

The cell wall of Gram-positive bacteria also carries teichoic acids (TAs). These glycopolymers are either attached to the PG (wall teichoic acids, WTAs) or anchored to the cytoplasmic membrane (lipoteichoic acid, LTAs) (Brown et al., 2013; Percy and Gründling, 2014). TAs are

* Corresponding author.
E-mail address: anne-marie.di-guilmi@cea.fr (A.M. Di Guilmi).
[1] Present address: Department of Biology, Indiana University, Bloomington, Indiana, USA.
[2] Present address: CEA, 18 route du panorama, 92265 Fontenay-aux-roses, France.

https://doi.org/10.1016/j.tcsw.2018.05.001
Received 23 March 2018; Received in revised form 17 May 2018; Accepted 18 May 2018
Available online 12 June 2018
2468-2330/

Table 1
Strains, plasmids and oligonucleotides used in this study.

Constructs	Genotype/description/sequence	Source
***S. pneumoniae* strains**		
R6		
R6 LytA-sfGFP	*bgaA::P_{cscD} –lytA (pJB3)*; Amp^R, Tet^R	This work
R6 ΔlytA	*lytA::cat*; Cat^R	Pagliero et al. (2008)
ΔlytA LytA-sfGFP	*lytA::cat, bgaA::P_{cscD} –lytA (pJB3)*; Cat^R, pJB3, Amp^R, Tet^R	This work
ΔlytA $LytAE_{87}Q$-sfGFP	*lytA::cat; bgaA::P_{cscD} –lytAE87Q (pJB31)*, Cat^R, Amp^R, Tet^R	This work
ΔlytA $LytA^{AMI}$-sfGFP	*lytA::cat; bgaA::P_{cscD} –lytA^{AMI}(pJB33);* Cat^R, Amp^R, Tet^R	This work
ΔlytA $LytA^{CBD}$-sfGFP	*lytA::cat; bgaA::P_{cscD} –lytA^{CBD}(pJB34);* Cat^R, Amp^R, Tet^R	This work
ftsZ-mKate	*R800 ftsZ::ftsZ-mKate*; Str^R	Bonnet et al. (2017)
RH426	*ΔcomA ΔIS1167*::Janus, Ery^RKan^R	Johnsborg and Håvarstein (2009)
RH1	*ΔcomA::ermAM, egb::spc*, Ery^R Spc^R	Johnsborg et al. (2008)
RH14	*ΔcomA::ermAM, egb::spc, ΔlytA::kan*, Ery^R Spc^R Kan^R	Eldholm et al. (2009)
SPH125	P_{comR}*::comR*, Janus between *cpsO* and *cpsN*, Ery^RKan^R	Berg et al. (2011)
SPH130	SPH125, but contains the P_1 and P_{comR} promoters before *comR*	Berg et al. (2011)
SPH131	SPH130, but with replacement of *luc* by the Janus cassette, Ery^RKan^R	Berg et al. (2011)
SPH143	SPH131 but with replacement of the Janus cassette by *tarIJ* (*spr1149/spr1148*), Ery^RSm^R	This work
SPH144	SPH143, but with replacement of native *tarI* and *tarJ* by the Janus cassette, Ery^RKan^R	This work
SPH145	SPH144, but with deletion of the Janus cassette, Ery^RSm^R	This work
SPH146	SPH145, but with replacement of *lytA* by a spectinomycin resistance marker (*aad9*), $Ery^RSm^RSpc^R$	This work
Plasmids		
pADG0	[*bgaA::P_{Zn}-sfgfpopt*], *Amp^R*, *Tet^R*, AgeI, BssHII, BsiWI	Bonnet et al. (2017)
pJB3	From pADG0, [*bgaA::P_{Zn}-LytA-sfgfpop*], *Amp^R*, *Tet^R*	This work
pJB31	From pJB3, [*bgaA::P_{Zn}-LytA^{E87Q}-sfgfpop*], *Amp^R*, *Tet^R*	This work
pJB33	From pJB3, [*bgaA::P_{Zn}-LytA^{AMI}-sfgfpop*], *Amp^R*, *Tet^R*	This work
pJB34	From pJB3, [*bgaA::P_{Zn}-LytA^{CBD}-sfgfpop*], *Amp^R*, *Tet^R*	This work
pADG12	From pET vector, 8-His-sfGFPop; Kan	This work
pADG14	8-His-sfGFPop-LytA; *Kan^R*	This work
pADG141	8-His-sfGFPop-$LytA^{AMI}$; *Kan^R*	This work
pADG142	8-His-sfGFPop-$LytA^{CBD}$; *Kan^R*	This work
pET28-His-LytA	pET28a::*his-lytA* Kan^R, Cm^R	Philippe et al. (2015)
pDS-lytA	pRSET A with *lytA* cloned downstream of *T7/lac*	Berg et al. (2011)
Oligonucleotides		
pJB3For	CGCGCGCGCATGGAAATTAATGTGAGTAAATTAAG	This work
pJB3Rev	GCGCGTACGTTTTACTGTAATCAAGCCATCTGG	This work
FORoMJ62	ggttgaatggctttcaatcagttgaaccgctgcataggtctcagc insertion of E87Q mutation in lytA	Bonnet et al. (2017)
REVoMJ63	gctgagacctatgcagcggttcaactgattgaaagccattcaacc insertion of E87Q mutation in lytA	Bonnet et al. (2017)
pJB33For	CAGTTTAAGCATGATATTGAGAACGGCTTGCGTACGACCGGTTCTAAAGGTGAAGAG	This work
pJB33Rev	CTCTTCACCTTTAGAACCGGTCGTACGCAAGCCGTTCTCAATATCATGCTTAAACTG	This work
pJB34For	GCGGATCTTAAGGAGGCGCGCATGACGATTGAAACAGGCTGGCAGAAG	This work
pJB34Rev	CTTCTGCCAGCCTGTTTCAATCGTCATGCGCGCCTCCTTAAGATCCGC	This work
pADG14For	CGCAAGCTT GAAATTAATGTGAGTAAATTAAGAAC	
pADG14REv	GCGCTCGAGTTATTATTTTACTGTAATCAAGCCATCTGG	
pADG141For	GCATGATATTGAGAACGGCTTGACTAATAACTC GAGCACCACCACCAC	This work
pADG141Rev	GTGGTGGTGGTGCTCGAGTTATTAGTCAAGCCGTTCTCAATATCATGC	This work
pADG142For	CCGAATTCGAGCTCCGTCGACAAGCTTGATTGAAACAGGCTGGCAGAAGAATG	This work
pADG142Rev	CATTCTTCTGCCAGCCTGTTTCAATCAAGCTTGTCGACGGAGCTCGAATTCGG	This work
khb31	ATAACAAATCCAGTAGCTTTGG	Berg et al. (2011)
khb36	TGAACCTCCAATAATAAATATAAAT	Berg et al. (2011)
khb33	TTTCTAATATGTAACTCTTCCCAAT	Berg et al. (2011)
khb34	CATCGGAACCTATACTCTTTTAG	Berg et al. (2011)
Kan484F	GTTTGATTTTTAATGGATAATGTG	Johnsborg et al. (2008)
LytAF	TGTATCTATCGGCAGTGTGAT	Eldholm et al. (2009)
LytAR	TCAACCATCCTATACAGTGAA	Eldholm et al. (2009)
khb90	ATTTATATTTATTATTGGAGGTTCAATGATTTATGCAGGAATTCTTGC	This work
khb91	ATTGGGAAGAGTTACATATTAGAAATTATACTTCCCACTTAAACACTG	This work
khb92	AGAGACCAGCATCAGGATAC	This work
khb93	CACATTATCCATTAAAAATCAAACCTATTTTCTCCTTTGTCTTAC	This work
khb94	AAGTATTTTCTAGTATTATAGCACATTTAACTTTCCTTATGCTTTTGGAC	This work
khb95	TTAAATGTGCTATAATACTAGAAAATACTTGTACTGGAGGTTAATTGTGGAG	This work
khb96	TTCACCTTGCTCTTCCTTATAG	This work
khb97	CTCCACAATTAACCTCCAGTACCTATTTTCTCCTTTGTCTTAC	This work
khb98	GTAAGACAAAGGAGAAAATAGGTACTGGAGGTTAATTGTGGAG	This work

important components of the cell wall and display numerous functions, in particular in cell morphology and cell division. In many bacterial species, like lactobacilli, bacilli and staphylococci, LTAs and WTAs display different chemical structures and their biosynthesis depends on distinct biochemical pathways. WTAs synthesis is controlled by *tag* and *tar* genes (Brown et al., 2013), while LtaS is a key enzyme in the LTAs biosynthesis pathway (Percy and Gründling, 2014; Grundling and Schneewind, 2007).

A functional link between TAs and PG hydrolases during cell division has been highlighted in *Bacillus subtilis* and *Staphylococcus aureus* (Yamamoto et al., 2008; Kiriyama et al., 2014; Schlag et al., 2010) but the molecular mechanisms of this interplay are still to be deciphered. Whether TAs control PG hydrolases by regulating their enzymatic activity and/or by playing a role in their subcellular localization are important issues. We addressed these questions in the context of the Gram-positive *Streptococcus pneumoniae* bacterium since pneumococcal TAs exhibit specific and convenient features relevant to this study. First, pneumococcal WTAs and LTAs chains have identical

repeated unit structures and length distribution, indicating that both polymers are produced by the same biosynthetic pathway (for review, see Denapaite et al., 2012). The second striking feature is the decoration of TAs by phosphorylcholine. The choline serves as an anchor for the class of Choline-Binding Proteins (CBPs), that include some PG hydrolases (Frolet et al., 2010). Their binding is non covalent and reversible, a property that allows easy manipulation of the system. Choline is not rare in bacteria but *S. pneumoniae* is the only known species whose growth entirely depends on exogenous choline which is exclusively integrated into the TAs. We recently took advantage of this choline growth dependency to label pneumococcal TAs with chemically-modified fluorescent choline molecules using a bioorthogonal reaction related to the click chemistry approach (Di Guilmi et al., 2017).

LytA belongs to the CBP family and is the major pneumococcal autolysin responsible for the autolysis that occurs several hours after entering the stationary phase (Tomasz, 1968; Howard and Gooder, 1974). LytA is a *N*-acetylmuramidase that cleaves between the d-lactate of Mur*N*Ac and the l-Ala which is the first residue in the stem peptide. LytA is only active against stationary-phase cells (Tomasz and Waks, 1975; Mellroth et al., 2012), suggesting that the arrest of the division process leads to PG sensitivity to LytA. We recently showed that PG O-acetylation also protects growing pneumococcal cells from lysis induced by LytA (Bonnet et al., 2017). In addition to the amidase catalytic domain, LytA contains a Choline-Binding Domain (CBD) that mediates the binding to TAs via the choline residues. This PG hydrolase is thus a relevant bivalent protein to exemplify the relationship between TAs and PG hydrolysis activity. Contrarly to most CBPs that contain an N-terminal signal peptide that targets them to the extracellular cell wall, LytA does not contain any recognisable motif for protein secretion (Frolet et al., 2010). This suggests that LytA should remain localized within the cytoplasm while its site of action is extracellularly. The mechanism(s) through which LytA reaches the cell wall are still unkown. One hypothesis involves programmed cell death (PCD), leading to membrane weakening and to the release of intracellular proteins. Alternatively, PCD could be induced by the production of H_2O_2 by SpxB leading to the release of LytA during the stationary phase (Regev-Yochay et al., 2007). PCD would also be involved in the release of pneumolysin, a potent cytotoxin also lacking a recognisable peptide signal, suggesting that H_2O_2 production by SpxB would induce the release of the pneumolysin during the exponential phase and of LytA during the stationary phase (Bryant et al., 2016).

We show here that during the stationary phase, LytA is released independently from its amidase activity while the cell lysis induced by LytA requires both enzymatic and TAs-binding functions. We also demonstrate that TAs are involved in the regulation of LytA activity. Firstly, the level of TAs present at the cell surface influences the sensitivity of growing pneumococcal cells to LytA and secondly, nascent TAs inserted at the division site are the specific receptors of LytA, tuning in this way the positioning of LytA at the cell surface.

Materials and methods

Plasmid construction and site-directed mutagenesis

Plasmids, and oligonucleotide primers used are listed in Table 1. The synthetic gene encoding the superfolder variant of GFP (sfGFPop) was optimized from the superfolder green fluorescent protein (sfGFP) variant (Pédelacq et al., 2006) for expression in *S. pneumoniae* (sfGFPop) and ordered from GeneArt (Invitrogen) (Bonnet et al., 2017). For the construction of pJB3 (Pzn-lytA-sfGFPop) plasmid, the *lytA* gene was amplified by PCR with pJB3For and pJB3Rev primers, digested by BssHII and BsiWI and inserted into pADG0 (Bonnet et al., 2017) between BssHII and BsiWI [bgaA::P_{czcD}-lytA-sfGFPop] to generate pJB3. pJB31 (Pzn-lytAE87Q-sfGFPop) plasmid was contructed by PCR-based site-directed mutagenesis using ForoMJ62 and RevoMJ63 primers to indroduce the E87Q mutation in the *lytA* on the pJB3 plasmid. pJB33 (Pzn-lytA^{AMI}-sfGFPop) plasmid was contructed by PCR-based site-directed mutagenesis using pJB33For and pJB33Rev primers to delete the choline binding domain sequence in the *lytA* on the pJB3 plasmid. pJB34 (Pzn-lytA^{CBD}-sfGFPop) plasmid was contructed by PCR-based site-directed mutagenesis using pJB34For and pJB34Rev primers to delete the amidase sequence in the lytA gene on the pJB3 plasmid. For the construction of the pADG12 plasmid, the gene encoding the superfolder GFP optimized for the expression in *S. pneumonia*e (sfGFPop) was cloned in a His tagged protein expression pET vector. For the construction of the pADG14 plasmid (8xHis-sfGFPop-LytA), the *lytA* gene was amplified by PCR with pADG14For and pADG14Rev primers, digested by HindHIII and XhoI and inserted into pADG12 between HindIII and XhoI to generate pADG14. pADG141 plasmid (8xHis-sfGFPop-LytA^{AMI}) was contructed by PCR-based site-directed mutagenesis using pJB141For and pJB141Rev primers to delete the choline binding domain sequence in the *lytA* gene on the pADG14 plasmid. pADG142 plasmid (8xHis-sfGFPop-LytA^{CBD}) was contructed by PCR-based site-directed mutagenesis using pJB142For and pJB142Rev primers to delete the choline binding domain sequence in the *lytA* gene on the pADG14 plasmid. DNA sequencing was performed by Beckman Coulter Genomics, Genewiz.

Bacterial strains

Strain SPH143 was derived from strain SPH131 (Berg et al., 2011) by replacing its Janus cassette (Sung et al., 2001) with the genes *tarI* and *tarJ* (*spr1149* and *spr1148*). The *tarIJ* fragment was amplified by PCR from *S. pneumoniae* RH1 using the primers khb90 and khb91. Fragments corresponding to the ~950 bp region upstream and ~800 bp region downstream of the Janus cassette in SPH131 were amplified using the primer pairs khb31/khb36 and khb33/khb34, respectively. These fragments were subsequently fused to the 5′ and 3′ ends of the *tarIJ* fragment using the primers khb31 and khb34 and overlap extension PCR as described by (Higuchi et al., 1988). The fusion product was used to transform SPH131, resulting in a strain that expresses *tarIJ* ectopically from P_{comX} when ComS* is added to the growth medium.

To construct the strain SPH144, the native *tarIJ* genes of strain SPH143 were replaced by the Janus cassette. The Janus cassette was amplified from RH426 using the primers Kan484F and khb94. Next, the primers khb92 and khb93 were used to amplify a ~800 bp DNA fragment corresponding to the region flanking the 5′ end of *tarI,* whereas the primers khb95 and khb96 were used to amplify the ~800 bp region flanking the 3′ end of *tarJ*. The two fragments were then fused to the 5′ and 3′ ends of the Janus cassette respectively, using the primers khb92 and khb96. Primer khb94 contains an overhang that introduced the synthetic constitutive promoter P_1 downstream of the Janus cassette. This ensured that the essential *licABC* genes, which are situated on the same transcriptional unit as *tarI* and *tarJ,* were still expressed when the Janus cassette was inserted in place of the *tarIJ* genes. During transformation and subsequent selection of transformants, ComS* (2 μM) was added to the growth medium and agar plates to drive ectopic expression of *tarIJ*. Strain SPH145 was constructed by deleting the Janus cassette in SPH144. Fragments corresponding to the ~800 bp upstream and downstream regions of the Janus cassette in strain SPH144 were amplified using the primer pairs khb92/khb97 and khb98/khb96. The fragments were joined using the primers khb92 and khb96, and the resulting fusion product was used to transform strain SPH144. This gave rise to strain SPH145, in which the regions flanking the native *tarIJ* genes are directly linked and normal expression of the *licABC* genes from their own promoter is re-established. Strain SPH146 was derived from SPH145 by replacing the *lytA* gene (*spr1754*) of SPH145 with a spectinomycin resistant marker (*aad9*). The *lytA*::Spc^R fragment used to transform SPH145 was amplified from the genome of RH431 using the primers LytAF and LytAR.

For the gene depletion studies of *tarIJ* we used the ComRS system described previously (Berg et al., 2011). In brief, strain SPH146 (*tarIJ*-depletion) was grown in the presence of 2 μM ComS*. The cells were collected by centrifugation and washed once in fresh C medium to remove excess ComS*. Then the cells were resuspended in fresh C medium without ComS* to an OD_{492} of 0.05 before they were twofold diluted in eppendorf tubes containing C medium. The dilution series were then transferred to a 96-well NBS clear-bottom plate (Corning) containing 2 μM or 0 μM ComS* and incubated in a FluoStar Optima plate-reader (BMG Labtech) at 37 °C. The OD_{492} was measured automatically every 10 min. In the experiments where expression of *tarIJ* was fine-tuned in a dose-dependent manner, cultures of SPH146 were diluted to OD_{492} ~ 0.05 in C medium with 2 μM ComS* and grown for 1 h. Then the cells were harvested, washed, and transferred to C medium containing a 1.25-fold dilution series of ComS* (0.125, 0.1, 0.08, 0.064, 0.0512, 0.041, 0.033 0.026 and 0.021 μM). Then the cells were transferred to a NBS clear-bottom plate for OD_{492}-measurments. When LytA-sensitivity was examined, LytA (5 μg ml^{-1}) was added to selected wells in the plate at the start of the experiment, or in the exponential growth phase at OD_{492} ~ 0.25.

WT lytA-sfGFP, ΔlytA-lytA-sfGFP, ΔlytA-lytAE87Q-sfGFP, ΔlytA-lytA^{AMI}-sfGFP and ΔlytA-lytA^{CBD}-sfGFP strains were obtained by transformation with pJB3 (*lytA-sfGFP*), pJB31 (*lytAE87Q-sfGFP*), pJB33 (-*lytA^{AMI}-sfGFP*) or pJB34 (*lytA^{CBD}-sfGFP*) plasmid (Tet^R), respectively in the appropriate genetic background. The strains, plasmids, and oligonucleotide primers used are listed in Table 1. Allelic replacements were performed using the Janus method, a two-step procedure based on a bicistronic kan-rpsL cassette called Janus (Sung et al., 2001). This method avoids polar effects and allows expression of the fusion proteins at physiological levels.

Growth conditions, media, and transformation

Liquid cultures of *S. pneumoniae* strains were grown at 37 °C/5%CO_2 in Cmedium (Cmed) supplemented with 0.5% yeast extract (Lacks and Hotchkiss, 1960) (CY), Chemically Defined Medium containing 5 or 10 μg/ml choline (CDM-Cho-5, CDM-Cho-10) or in Todd Hewitt medium (TH; BD Sciences). For strains harboring a zinc-inducible plasmid, CY was supplemented with 0.15 mM $ZnCl_2$ to induce protein expression. For transformation, about 250 ng of DNA was added to cells treated with synthetic competence stimulating peptide 1 in TH medium at pH 8.0 supplemented with 1 mM $CaCl_2$. Cells were grown for 2 h at 37 °C/5%CO_2, and transformants were selected on Columbia (BD Sciences) blood (4%) agar plates containing the appropriate antibiotics (tetracyclin 250 μg/ml).

Continuous growth was followed by inoculating 2.5 ml of CY, CDM-Cho-5 or CDM-Cho-10 in 24-wells plates, which were sealed and incubated at 37 °C in a FLUOstar plate reader (BMG Labtech) equipped with a 595-nm filter. The OD_{595} was recorded every 10 to 20 min after shaking. Each point was done in triplicate and experiments repeated three independent times. LytA sensitivity was determined by adding the recombinant His-LytA at 10 μg/mL at OD_{595nm} 0.3–0.4.

The localizations of sfGFPop-LytA, sfGFPop-LytA^{AMI} and sfGFPop-LytA^{CBD} were performed as follow: the recombinant proteins were added at 10 μg/ml in CY pneumococcal cultures at $OD_{595\,nm}$ 0.3–0.4. The incubations lasted from 4 min to 30 min at room temperature. After two washes in CY to discard unbound fluorescent proteins, the cells were resuspended into CY and immediately observed.

For labeling of newly synthesized PG, cells were grown in CY at $OD_{595\,nm}$ 0.4 at 37 °C/5%CO_2, pelleted at room temperature for 2 min at 4500 g, resuspended and incubated for 3 min in CY supplemented with 2 mM HADA (Kuru et al., 2012). After two washes in CY to discard unbound dye, the cells were resuspended into CY and immediately observed.

For pulse-labelling of newly synthesized teichoic acids, cells were grown in Cmed supplemented with 4 μg/ml choline at 37 °C/5%CO2 until $OD_{595\,nm}$ 0.4, then pelleted at room temperature for 2 min at 4500 g, resuspended and incubated for 5 min in Cmed supplemented with 4–10 μg/ml choline-alkyl (manuscript submitted) and 25 μM DIBO (Click-IT™ Alexa Fluor™ 594 DIBO Alkyne, for copper free click chemistry detection of azide – C10407). After two washes in Cmed to discard unbound dye, the cells were resuspended into CY and immediately observed.

In pulse-chase experiment, pulse-labelling of newly synthesized teichoic acids was performed as described in the above paragraph. sfGFPop-LytA recombinant protein at 10 μg/ml was added at the same time than the choline-alkyl and DIBO molecules. After resuspension into CY and immediate observation of a first aliquot (time 0), cells were incubated at 37 °C/5%CO2 and aliquots were observed after 20 and 40 min.

Protein expression and purification

Strain BL21(*DE3*) Rosetta pLysS Rare (Cm^R) of *E. coli* was transformed with the plasmids pET28-His-LytA (Kan^R), pADG14 (Kan^R), pADG141 (Kan^R), or pADG142 (Kan^R). Cells were grown in Luria Bertani medium and protein expression was induced at OD_{595nm} 0.6 with 0.5 mM IPTG (isopropyl β-*D*-thiogalactopyranoside) at 25 °C overnight. Cells from 2-litres cultures were harvested by centrifugation, resuspended in 50 ml of a buffer containing 50 mM Tris pH 8.0, 500 mM NaCl, 25 mM imidazole, 10% glycerol and a protease inhibitor cocktail (Complete EDTA free, Sigma–Aldrich) and lyzed using a Microfluidize M-110P (Microfluidics). The lysate was clarified by centrifugation (20 min at 39,191 × *g* at 4 °C) and loaded onto a 10-ml Ni-nitrilotriacetic acid (NTA) column (Qiagen). His-LytA proteins were eluted with a 25 mM to 500 mM imidazole gradient. Pooled fractions were concentrated and further purified by size exclusion chromatography using a Superdex S75 10/300 GL column (GE Healthcare) in 25 mM Tris-HCl (pH 8) and 150 mM NaCl.

Fluorescence microscopy image acquisition and analysis

Cells were grown at 37 °C/5%CO_2 in CY to $OD_{595\,nm}$ 0.3, transferred to microscope slides, and observed at 37 °C on an Olympus BX61 microscope equipped with a UPFLN 100O-2PH/1.3 objective and a QImaging Retiga-SRV 1394 cooled charge-coupled-device camera or an Olympus IX81 microscope equipped with a UPFLN 100O-2PH/1.3 objective and a Hamamtsu Orca Flash4 camera.

Image acquisition was performed using the software packages Volocity. Images were analyzed using the open-source softwares MicrobeTracker (Sliusarenko et al., 2011) and Oufti (Paintdakhi et al., 2016) and processed with Adobe Photoshop CS5 and Image J. Demographs integrate the signal values in each cell. The cells were sorted by their length value and the fluorescence values were plotted as a heat map.

Time lapse microscopy was performed using the automated CellASIC ONIX Microfluidic Platform (EMD Millipore Corporation). Briefly, a glycerol stock of WT strain was inoculated in 5 ml of CY medium and grown to an OD_{600nm} of 0.05. Bacterial cells were loaded into an ONIX B04A-03 microfluidic plate (EMD Millipore Corporation) at 0.25 psi and a constant flow of CY medium at 1 psi was subsequently applied during 1 h. A rapid injection of sfGFPop-LytA recombinant protein at 50 μg/mL was done during 10 min at 3 psi followed by a washing of 5 min at 2 psi, then the flow was reduced to 0.25 during the chase. Images were acquired every 5 min during 1 h using an automated inverted epifluorescence microscope Nikon Ti-E/B equipped with the "perfect focus system" (PFS, Nikon), a phase contrast objective (CFI Plan Apo Lambda DM 100X, NA1.45), a Semrock filter set for GFP (Ex: 482BP35; DM: 506; Em: 536BP40) a LED light source (Spectra X Light Engine, Lumencor), a sCMOS camera (Neo sCMOS, Andor) and a chamber thermostated at 37 °C. Fluorescence images were capturated and processed using Nis-Elements AR software (Nikon). GFP

fluorescence images were false colored green and overlaid on phase contrast images.

CBP elution by 2%choline and LytA quantification by immunoblotting

For quantification of the cell-wall anchored LytA, cells were grown at 37 °C in 50 ml of filtered CY and every 40 min, the OD_{595nm} was measured and culture samples of 1 ml were withdrawn. The cells were centrifigated for 2 min at 5000 g and the pellet was resuspended into 10 µl of CY containing or not 2% Choline (Yother and White, 1994). After an incubation period of 20 min under gentle mixing, the samples were centrifugated for 3 min at 5000 g and the supernatant containing the CBP eluted by 2% choline was withdrawn. Fractions treated and non-treated with choline were analyzed by immunoblot and quantified with ImageJ. The samples were boiled in Laemmli for 5 min, loaded on SDS-PAGE gel and run at 200 V for 30 min. The gel was transferred to a nitrocellulose membrane which was then blocked with 5% milk in PBS-T (phosphate-buffered saline with 0.1% Tween) (saturation solution) for 1 h at room temperature. The membrane was incubated with an anti-LytA polyclonal rabbit antibody diluted in the saturation solution for 1 h at room temperature. After three washes in PBS-T, the membrane was incubated with a goat anti-rabbit immunoglobulin coupled to the G-horseradish peroxidase) for 1 h30 at room temperature. Protein was detected with the ECL horseradish peroxidase Western blotting detection kit. Quantitative analysis was realized with ImageJ.

Sacculi purification and transmission electron microscopy

Sacculi from *S. pneumoniae* R6 strain were prepared as described previously (McPherson and Popham, 2003). 10 µL of sacculi were incubated at 37 °C for 1 min with 0 (Control) or 5 µg/mL of recombinant purified LytA for 1 min at 37 °C in 100 µL PBS. Samples were then applied to the clean side of carbon on mica (carbon/mica interface) and negatively stained with 2% (wt/vol) sodium silicotungstate (pH 7.4). A grid was placed on top of the carbon film, which was subsequently air-dried. Images were taken under low dose conditions with a CM12 Phillips electron microscope at 120 kV and a calibrated nominal magnification of 13,000 using an ORIUS SC1000 camera (Gatan, Inc.).

Scanning and transmission electron microscopy

To deplete *tarIJ* in SPH146 cells, ComS* was removed from the growth medium as described by Berg et al. (2013). During depletion, growth was followed spectrophotometrically, and 25 ml samples of cell culture were collected when the growth rate of the *tarIJ*-depleted cells were significantly reduced compared to SPH146 cells grown in the presence of 2 µM ComS*. The collected cells were fixed and prepared for SEM and TEM as described previously (Straume et al., 2017).

Results

Reduced choline concentration in the culture medium triggers sensitivity to LytA in growing pneumococci

To test if TAs would drive the activity of LytA, we first asked whether the pattern of TAs associated to the cell wall, or the level of choline decoration, might affect PG sensitivity to LytA. *S. pneumoniae* cells were cultured in media containing different concentrations of choline. CY medium (C-medium supplemented with 0.5% of yeast extract) contains a concentration of choline superior to 5 µg/ml, indeed, the C-medium contains 5 µg/ml of choline but the quantity of choline present in yeast extract is unknown. To control the concentration of choline, Chemically-Defined Medium (CDM) was prepared and supplemented with 5 µg/ml or 10 µg/ml of choline, CDM-Cho-5 and CDM-Cho-10 conditions, respectively. Growth rates in these media are reduced compared to CY medium (Fig. 1A, B, C, black curves). The most important effect is observed in CDM-Cho-5 (Fig. 1C, black curve) since exponential phase ended at $OD_{600\,nm}$ 0.8 compared to $OD_{600\,nm}$ 1.2–1.4 in CY and CDM-Cho-10.

As shown by other investigators and ourselves (Tomasz and Waks, 1975; Mellroth et al., 2012; Bonnet et al., 2017), the presence of exogenous LytA in pneumococcal culture does not affect the exponential growth phase rate but accelerates the onset of the lytic phase (Fig. 1A, grey curve). These experiments were performed with the pneumococcal wild-type strain to compare the lytic effect of exogenous LytA in respect to the endogenous one. We then investigated whether the concentration of choline in the medium would influence the sensitivity of growing cells to LytA. Pneumococcal cultures grown in CDM-Cho-10 and CDM-Cho-5 were supplemented with LytA (10 µg/ml final concentration) at mid-exponential phase ($OD_{600\,nm}$ 0.5) (Fig. 1B and C, grey curves). Immediately after addition of LytA, the growth rate dropped for about 30 min in both conditions and resumed in CDM-Cho-10 but not in CDM-Cho-5 where total cell lysis occurred. These data suggest that the quantity of choline present in the culture medium affects the sensitivity of PG to LytA cleavage. These results also suggest that choline starvation might lead to the production of TAs displaying a decreased level of choline decoration or to a reduced amount of TAs exposed at the cell surface, since only TAs substituted with choline are exported to the cell surface (Damjanovic et al., 2007).

Reduced expression of tarIJ triggers LytA sensitivity in growing pneumococci

To test this second hypothesis, *i.e.*, whether the amount of TAs at the cell surface would influence the sensitivity of pneumococcus to LytA, we used a depletion system to construct a mutant strain *tarIJ*, in which the amount of TAs produced can be controlled by the extracellular concentration of an 8-amino acid peptide designated ComS* (Berg et al., 2011). The genes, *tarI* and *tarJ* encode a ribitol 5-phosphate cytidylyl transferase and a ribulose 5-phosphate reductase, both required for the synthesis of the TAs precursor cytidine 5′-diphosphate (CDP)-ribitol (Baur et al., 2009). When CDP-ribitol is no longer available in the cell, WTAs and LTAs syntheses stop, resulting in growth arrest and cell death. The depletion of the *tarI* and *tarJ* genes was performed in a pneumococcal strain deleted for *lytA* (SPH146). Depletion of *tarIJ* alters the sensitivity of pneumococci to LytA (see below), and the presence of endogenously produced LytA might therefore influence the results of our experiments. First, the lowest ComS* concentrations that supports normal or nearly normal growth of the SPH146 strain were determined. When grown in the presence of 2 µM ComS*, the strain SPH146 grew normally and showed normal morphology (Fig. 2A and D). SPH146 cells grown in the presence of 2 µM ComS* were harvested by centrifugation, washed once with plain medium and resuspended to $OD_{492\,nm}$ 0.05 in the same medium containing concentrations of ComS* ranging from 0.04 to 0.125 µM (Fig. 3A). Cultures grown in medium containing 0.1 µM and 0.125 µM ComS* grew well whereas cultures containing lower concentrations of ComS* displayed impaired growth (Fig. 3A). TAs-depleted cells developed an elongated shape and appeared to have several septa (Fig. 2B and C). Transmission electron microscopy revealed that they contained several false or aborted septa initiations, demonstrating that they struggled to divide (Fig. 2E). These results show that TAs play a crucial role in septum formation in *S. pneumoniae*.

The LytA sensitivity of *tarIJ*-depleted cells was investigated by adding exogenous LytA to exponentially growing cultures at $OD_{492\,nm}$ 0.25. As expected, *tarIJ* cells grown at the highest ComS* concentration (0.125 µM) were resistant to LytA during exponential phase, while those grown at 0.08 µM were sensitive (Fig. 3B). At 0.1 µM only a portion of the cells was affected when LytA was added at OD_{492nm} 0.25, but after reaching OD_{492nm} 0.45 the whole culture lysed. These experiments indicate that actively growing pneumococci are sensitive to exogenous LytA when the amount of TAs in their cell envelope is reduced to a critical level. We have previously demonstrated the effect of

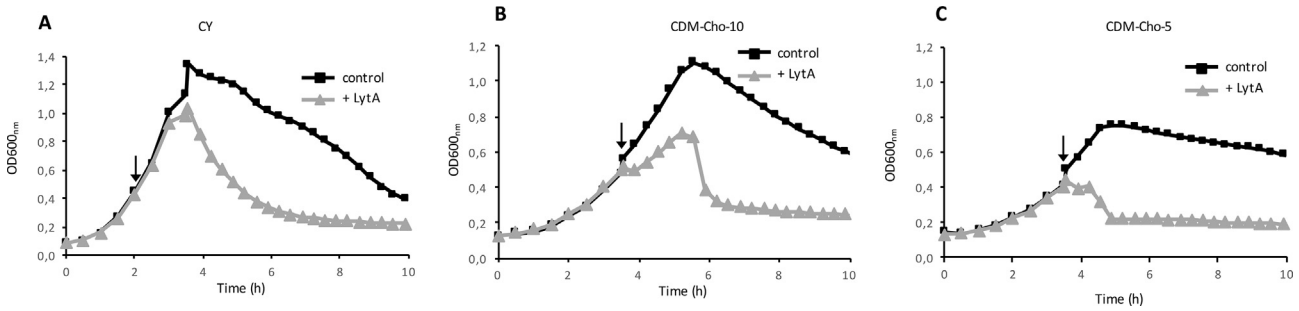

Fig. 1. Effect of choline on pneumococci sensitivity to LytA-induced lysis. A. Growth of wild-type pneumococci in CY, a choline-rich medium, in the absence or in the presence of exogenous LytA at 10 µg/ml. B. Growth in CDM medium, containing a choline concentration of 10 µg/ml, in the absence or in the presence of exogenous LytA at 10 µg/ml. C. Growth in CDM medium, containing a choline concentration of 5 µg/ml, in the absence or in the presence of exogenous LytA at 10 µg/ml. The addition of exogenous LytA is indicated by an arrow in all three panels.

MurNAc O-acetylation on the formation of robust and mature PG and in the protection of PG from LytA activity (Bonnet et al., 2017). These results, together with the data presented here, indicate that the structure of PG (probed by the accessibility of the Mur*N*Ac – l-alanine amide bond to LytA) shoud depend on both the MurNAc O-acetylation and the level of TAs present at the cell surface.

Localization of LytA varies according to pneumococcal growth phase

The data obtained so far indicate that the amount of TAs in the cell wall affects the lytic activity of LytA. We next asked if this effect could be correlated to TAs and LytA respective distribution at the cell surface. We first analyzed the cellular localization of LytA over the cell cycle.

The 5′ end of the *lytA* gene was fused to the superfolder green fluorescent protein optimized for expression in *S. pneumoniae* (sfGFPop) (Fig. S1A) and placed under the control of a Zn-inducible promoter (Eberhardt et al., 2009). Pneumococcal *lytA* mutant strain carrying the construction LytA-sfGFPop was grown in the presence of Zn. Expression level of the ectopic copy of *lytA* induced by Zn is lower than the endogenous expression level (Fig. S1B) as already observed for other pneumococcal genes (Eberhardt et al., 2009; Morlot et al., 2013). Although added at low concentration (0.15 mM), addition of Zn accelerates the onset of cell lysis (Fig. S1C, grey curves). As expected, the mutant strain deleted for *lytA* does not display lytic phase, independently of the presence of Zn (Fig. S1D). In the complemented strain, the expression of LytA-sfGFPop restored the lytic phase, although to a lesser extend than in the *lytA* mutant strain considering the LytA lower expression level induced by Zn compared to the endogenous *lytA* gene (Fig. S1D). Altogether, these data indicate that the expression of an ectopic copy of LytA fused to sfGFPop is functional in pneumococcal cells. The phenotype of the cells expressing LytA-sfGFPop was analyzed in a *lytA* deletion background to ascertain that the localization and lytic effect observed raised only from the LytA-sfGFPop, excluding then any side effect generated by the endogenous LytA.

We monitored the localization of LytA-sfGFPop at different phases of the pneumococcal growth by epifluorescence microscopy (Fig. 4A). LytA-sfGFPop appeared homogenously localized in the cytoplasm of growing cells (exponential phase) but concentrated into foci in cells that stopped growing (stationary phase), referred hereafter as “heterogeneous protein organization”. Surprisingly, during the lytic phase, all the intact cells exhibited discrete LytA-sfGFPop labeling at mid-cell. Quantification of the fluorescence distribution indicate that all growing

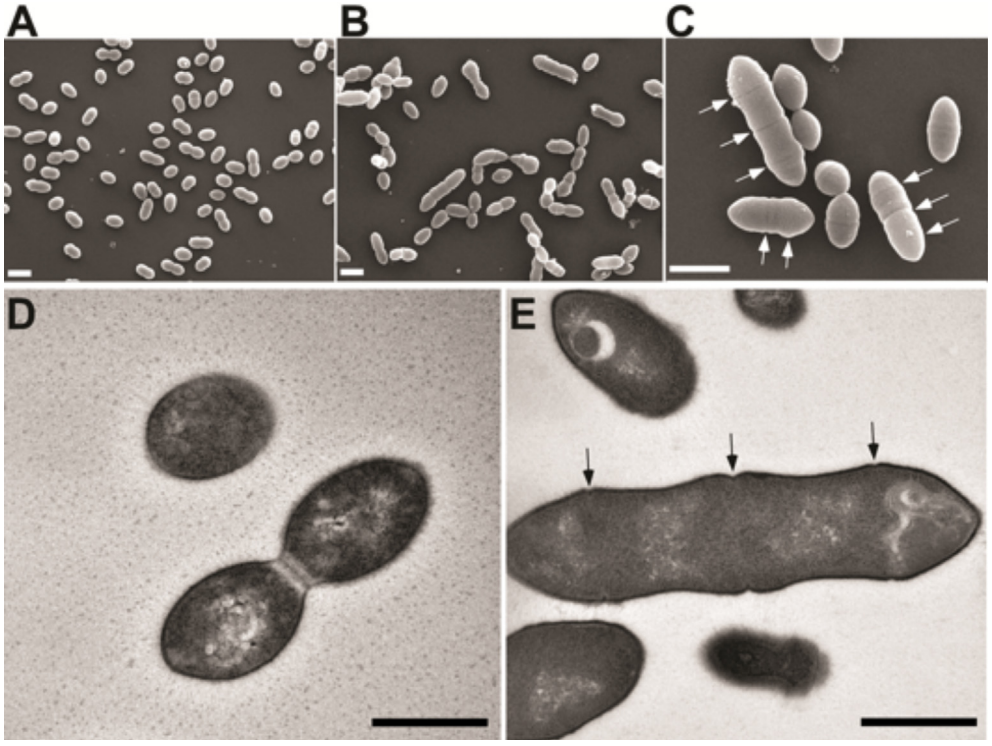

Fig. 2. Scanning (A, B and C) and transmission (D and E) electron micrographs of normal (A and D) and *tarIJ* depleted (B, C and E) *S. pneumoniae* cells. Cells grown in the presence of 2 µM ComS* (A and D) displayed the typical ovococcal shape of wild-type pneumococci. Depletion of *tarIJ* expression by removal of ComS* from the growth medium (B, C and E) gave rise to severe morphological abnormalities and multiple false or aborted division zones (indicated by arrows). All cell samples were collected during exponential growth. Scale bars in A, B, C: 1 µm; in D and E: 0.5 µm.

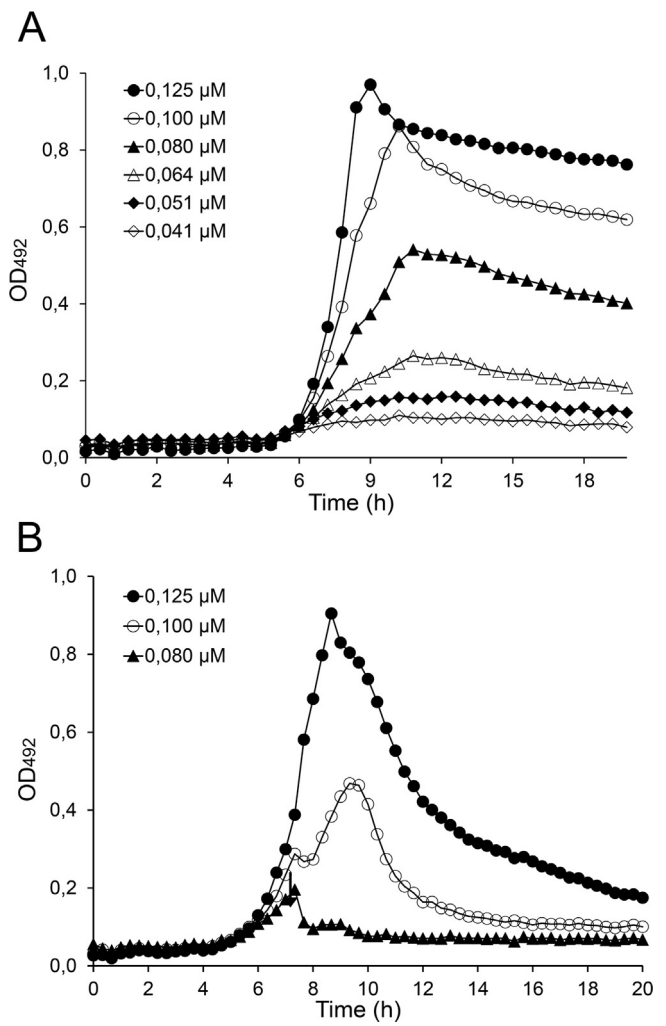

Fig. 3. Reduced expression of *tarIJ* triggers LytA sensitivity in growing *S. pneumoniae*. A. Impact of decreasing TarIJ expression on the growth of SPH146. TarIJ expression was regulated by growing the SPH146 cells in medium containing concentration of ComS* ranging from 0.125 to 0.041 µM. B. LytA-sensitivity of SPH146 cells growing exponentially in medium containing 0.125, 0.100 and 0.080 µM ComS*. Purified LytA (5 µg ml^{-1}) was added to the cultures when they reached OD_{492} 0.2–0.3, as indicated by the arrow.

cells display the homogenous LytA labeling (Fig. 4B). The proportion of this cell population decreases during the stationary growth phase in favour to an increasing amount of cells harboring the heterogeneous LytA pattern. During the lytic phase, LytA is positioned at mid-cell in the large majority of non-lyzed cells. The representation of the fluorescence signal profile arranged by increasing cell length (demograph) of a growing cell population and of cells withdrawn during the lytic phase illustrate the homogenous and the mid-cell patterns of LytA-sfGFPop (Fig. 4C).

LytA released in the medium binds to the surface of neighboring cells at mid-cell position

To test the subcellular localization of LytA (cytoplasmic or extracellular), cells were incubated with 2% choline, a quantity of choline sufficient to elute CBPs (like LytA) from the cell surface (Yother and White, 1994). Cells were withdrawn in lytic phase and the percentage of homogenous, heterogeneous and mid-cell fluorescence signal provided by the expression of LytA-sfGFPop was determined before and after treatment with 2% choline (Fig. 5A). Total loss of the mid-cell pattern after choline treatment was observed while the heterogeneous profile remained unchanged. These results reveal that LytA-sfGFPop positioned at mid-cell is extracellularly exposed in contrast to the heterogeneous pattern, which corresponds to a cytoplasmic localization. After choline treatment, we observed that all cells still exhibited fluorescence suggesting that cells with a surface fluorescent signal still contain cytoplasmic LytA-sfGFPop. LytA-sfGFPop release arises at the end of the linear growth phase (Fig. S2) and it significantly increases during the lytic phase reaching up to 20% of the total protein expressed, in accordance with published results (Mellroth et al., 2012).

To test whether extracellular LytA remains associated to the "exporter" cell or binds to sibling cells, cells expressing LytA-sfGFPop and cells expressing FtsZ fused to a red fluorescent protein (FtsZ-mKate2) were grown to mid-exponential phase and mixed to a ratio of 2:1. Growth of the mixed cultures was pursued at 37 °C until the lytic phase was reached. Imaging of the mixed populations showed that LytA-sfGFPop was associated to FtsZ-mKate2 expressing cells indicating that LytA-sfGFPop associates in *trans* to sibling non-lyzed cells (Fig. 5B).

Release of LytA is independent of the lytic activity but both amidase and CBD domains are required

We addressed the question of the molecular determinants responsible for the release and the lytic activity of LytA in pneumococcal cells. To do so, different variants of LytA fused to sfGFPop were expressed in the Δ*lytA* mutant strain and the growth profiles of each strain were analyzed. As expected, the inactive form LytAE_{87}Q-sfGFPop did not complement the lytic phenotype, confirming that the enzymatic activity of LytA is necessary to induce cell lysis (Fig. 5C). However, this strain displayed the same 3-phases localization pattern as the wild-type strain (Fig. S3). To further investigate the functional properties of LytA, the amidase (Ami) and CBD domains were individually fused to sfGFPop and expressed in the Δ*lytA* mutant strain. Neither LytA^{AMI}-sfGFPop nor LytA^{CBD}-sfGFPop were able to induce cell lysis (Fig. 5D, 5E). Altogether, these data indicate that i), the release of LytA is not dependent from the amidase enzymatic activity and ii), LytA should be anchored to TAs by the CBD to exert cell lysis function.

LytA localization at the cell surface is driven by the CBD

Since the lytic activity of LytA is dependent on its binding to TAs, we analyzed the molecular determinants driving the localization of LytA at the cell surface. To do so, we exploited the property of the CBPs to associate to TAs when added exogenously to pneumococcal cells. The full-length LytA and the individual CBD and amidase domains were fused to the sfGFPop at the N-terminal ends and expressed in *Escherichia coli*. The recombinant proteins sfGFPop-LytA (Fig. S1A), sfGFPop-LytA^{CDB} and sfGFPop-LytA^{AMI} were purified to homogeneity. No amidase activity was detected in the fusion sfGFPop-LytA probably because the catalytic domain is constrained by the sfGFPop proximity. We took advantage of this feature to focus only on the binding property of LytA and not on the cleavage of the PG Mur*N*Ac – l-alanine amide bond. The fluorescent proteins were tested for their ability to associate to growing pneumococcal cells (Fig. 6A). No binding of sfGFPop-LytA^{AMI} was observed confirming that the isolated catalytic domain is unable to attach to the cell surface (data not shown). The protein sfGFPop-LytA^{CBD} was shown to associate to the cell surface with a pattern similar to the one of the full-length sfGFPop-LytA (Fig. 6A). The demograph representations of the signal profiles of sfGFPop-LytA and sfGFPop-LytA^{CBD} in cells arranged by increasing cell length clearly show a localization at mid-cell as well as at a single pole (Fig. 6A). These data indicate that TAs recognition depends on CBD and that the specific localization of LytA is only dependent on the TAs-CBD interaction. We then sought to analyze the localization pattern of LytA in relation with its enzymatic activity. Purified sacculi prepared from pneumococcal growing cells were purified and digested with recombinant LytA (Fig. 6B). Electron microscopy observations indicate that cleavage of the sacculi occurred at the

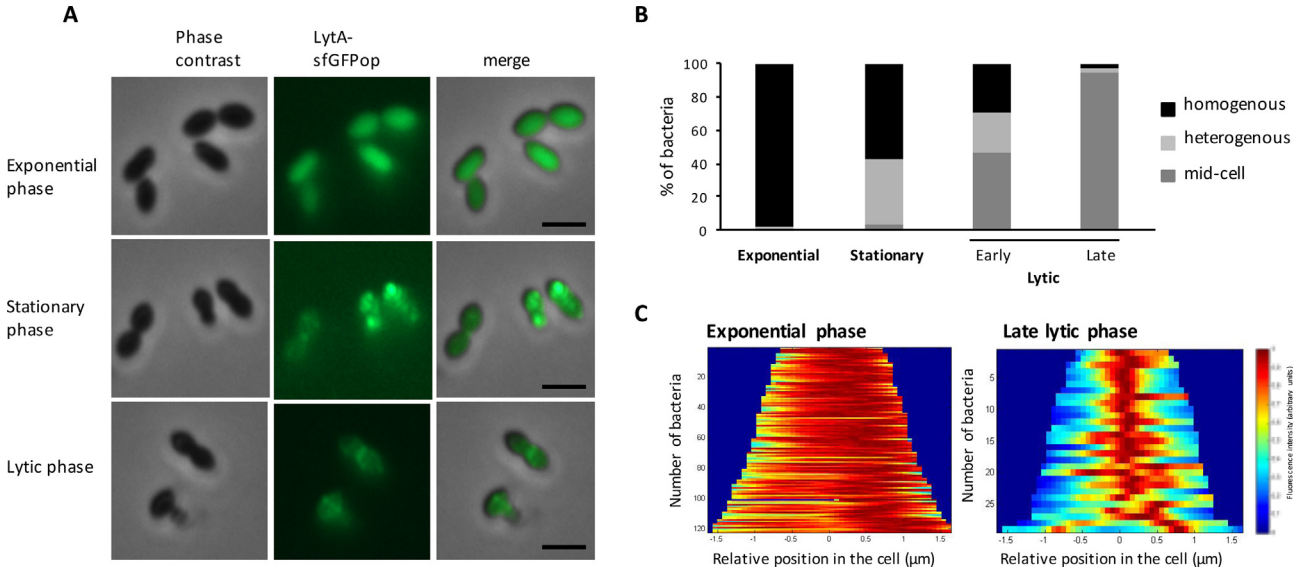

Fig. 4. Localization of LytA varies according to the culture growth phase. A. Fluorescence images of LytA-sfGFPop expressed in Δ*lytA* cells withdrawn at different growth phase. Phase contrast (grey), GFP fluorescent signal (green) and merge (right) images are shown. Scale bars: 2 µm. B. Distribution of bacteria displaying homogeneous, heterogeneous and mid-cell localization of LytA-sfGFPop during exponential phase ($OD_{600\,nm}$ 0,40), stationary phase ($OD_{600\,nm}$ 0,97), early ($OD_{600\,nm}$ 0,76) and late ($OD_{595\,nm}$ 0,23) lytic phase. N = 98–170 bacteria per OD point were analyzed. C. Demograph representation of the fluorescence signal profile of LytA-sfGFPop in cells sorted by increasing cell length (MicrobeTracker, MATLAB). Images analysis was performed on cells withdrawn during the exponential phase (upper demograph) and the late lytic phase (bottom demograph). N = 30–120 bacteria per demograph were analyzed.

mid-cell and polar sites, which correspond to the positions occupied by sfGFPop-LytA on live growing cells.

In non-growing cells withdrawn in stationary phase, sfGFPop-LytA positions only at mid-cell corresponding to the former site of active cell wall synthesis (Fig. S4), a pattern reminiscent to the one observed with the endogenous form of fluorescent LytA when bound to neighbouring non-lyzed cells (Fig. 5B). Although neither TAs nor PG are synthesized during stationary phase, LytA might keep the capability to recognize TAs species formerly synthesized during the exponential phase.

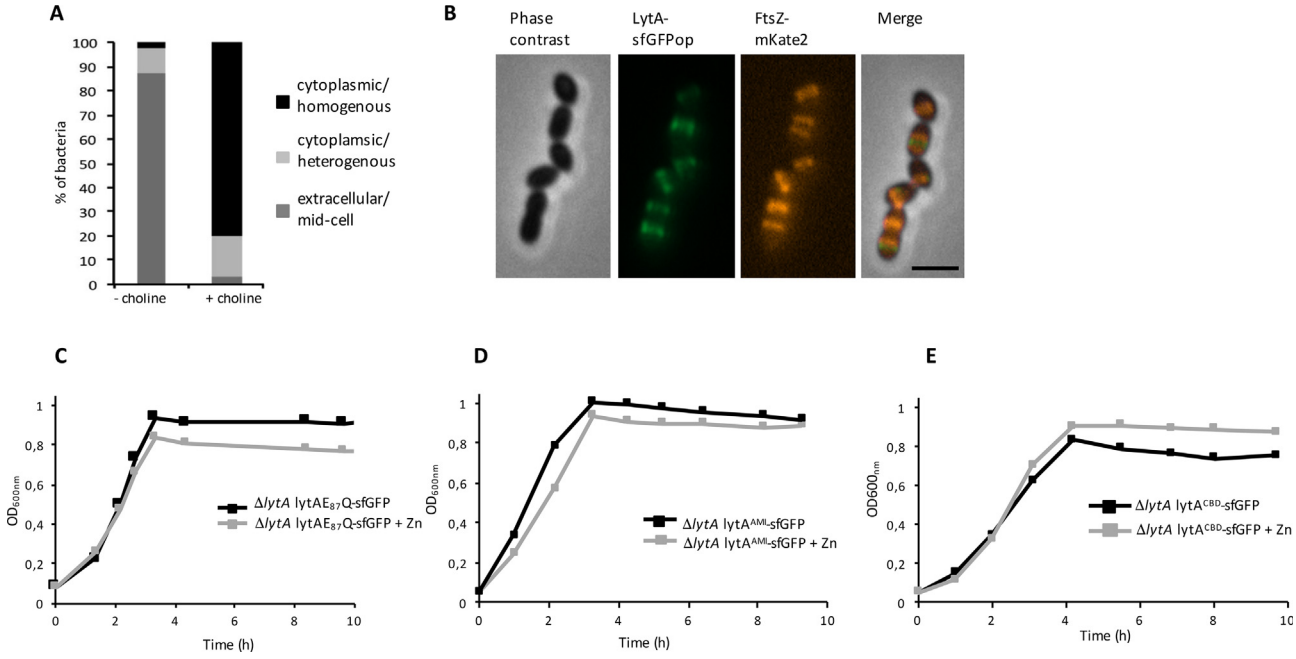

Fig. 5. LytA is released in the medium and binds at the surface of non-lyzed cells at mid-cell. A. Distribution of bacteria displaying homogeneous, heterogeneous and mid-cell localization of LytA-sfGFPop during lytic phase before and after treatment with 2% choline. B. Pneumococcal wild-type cells expressing LytA-sfGFPop were mixed with cells deleted from *lytA* and expressing FtsZ fused to a red fluorescent protein (mKate2) at the ratio 2:1. The growth of the mixed culture was pursued at 37 °C until and aliquots were withdrawn when the culture entered the lytic phase. Phase contrast (grey), GFP fluorescent signal (green), mKate2 (red) and merge (right) images are shown. Scale bars: 2 µm. C. Growth curves of the Δ*lytA* strain transformed with the Zn-inducible plasmid encoding the inactive form of LytA, $LytAE_{87}Q$, in the absence or the presence of 0.15 mM Zn. D. Growth curves of the Δ*lytA* strain transformed with the Zn-inducible plasmid encoding the amidase domain of LytA, in the absence or the presence of 0.15 mM Zn. E. Growth curves of the Δ*lytA* strain transformed with the Zn-inducible plasmid encoding the CBD domain of LytA, in the absence or the presence of 0.15 mM Zn. (For interpretation of the references to colour in this figure caption, the reader is referred to the web version of this article.)

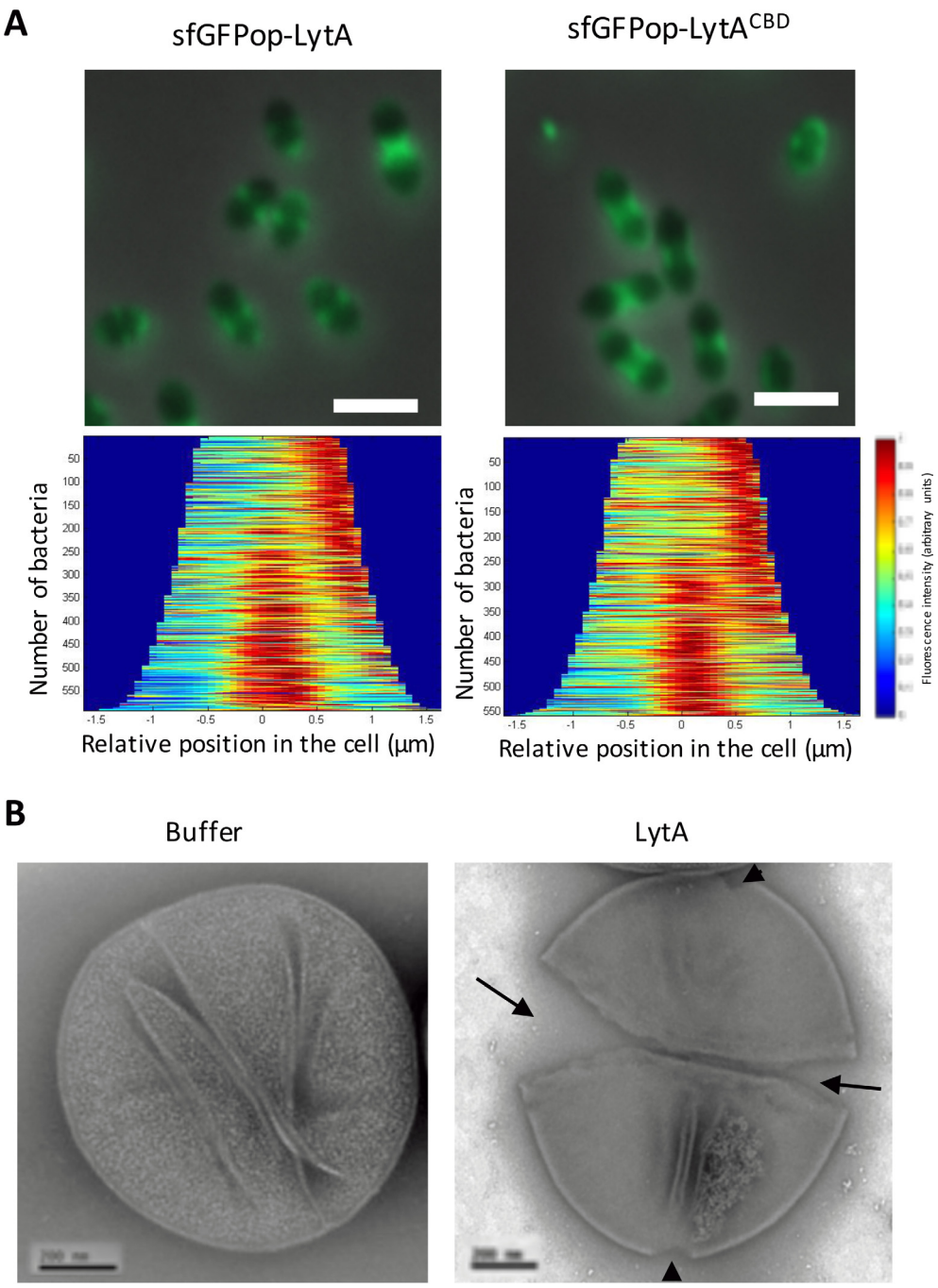

Fig. 6. Localization of LytA and cell wall cleavage sites. A. The CBD is sufficient to trigger localization of LytA. Wild-type cells in exponential growth phase were incubated with sfGFPop-LytA or sfGFPop-LytA^{CBD} recombinant proteins (10 µg/mL). Merge image of fluorescence and phase contrast views are showed. Scale bars: 2 µm. Demograph representation of the signal profile of sfGFPop-LytA and sfGFPop-LytA^{CBD} in cells sorted by increasing cell length (MicrobeTracker, MATLAB). B. Electron micrographs of *S. pneumoniae* sacculi incubated 1 min at 37 °C with buffer or with 5 µg/mL of recombinant purified LytA. Cleavage of the cell wall by LytA at both sides of the mid-cell sites are indicated by arrows and at the cell pole by arrow heads.

LytA binds to newly synthesized cell wall

To investigate in more details the distribution pattern of LytA at the cell surface, we followed the position of the division machinery using FtsZ-mKate2 and of the regions of active PG synthesis using labelled D-amino acids (HADA) (Kuru et al., 2012) together with the localization of sfGFPop-LytA. Of note, the morphogenetic process of ovococcal bacteria like *S. pneumoniae* is distinct from that of cocci like *S. aureus* and rod-shape organisms exemplified by *B. subtilis* since it results from two modes of PG insertion, one allowing division by synthesizing a septum (septal or cross-wall synthesis), the other allowing elongation by synthesizing peripheral cell wall (peripheral synthesis). sfGFPop-LytA and HADA were added to cells expressing FtsZ-mKate2. The incubation lasted for 4 min before washing and observation (Fig. 7). At the pre-division stage (i), FtsZ-mKate2 is positioned at the mid-cell site although no PG has been yet synthesized and sfGFPop-LytA is mainly detected at one cell pole. The early division stage (ii) is launched when cross-wall PG synthesis at the division site initiates cell constriction, this septal site is also occupied by FtsZ-mKate2 and sfGFPop-LytA. As the peripheral growth progresses (iii), sfGFPop-LytA is still present at the septal site, probably on both sides of the cross-wall site since the labeled zone appears slightly enlarged. FtsZ-mKate2 is then repositioned at the equator of the daughter cells which is the future site of division (iv) before *de novo* association of sfGFPop-LytA and HADA to these new division sites (v). In the meantime, a population of sfGFPop-LytA remains associated to the former parental division site, which corresponds to the new poles of the daughter cells (v).

We also investigated in real-time the localization of sfGFPop-LytA during cell division in a microfluidic system. sfGFPop-LytA was pulse-injected on cells before extensive wash with CY medium. The

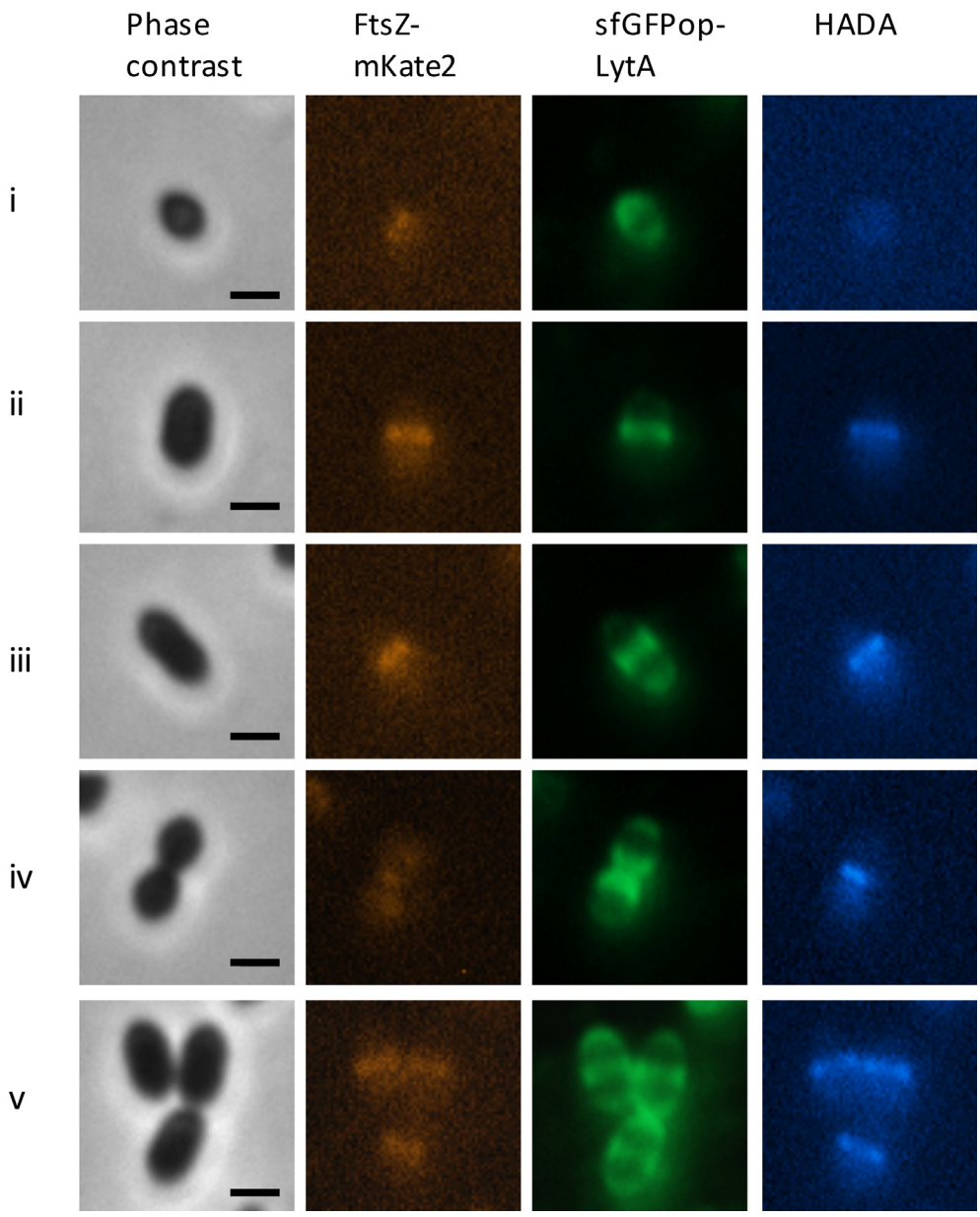

Fig. 7. LytA is associated to newly synthesized cell wall in growing cells. sfGFPop-LytA (10 µg/ml) and fluorescent amino-acid HADA (500 µM) were added to pneumococcal cells ($OD_{600\,nm}$ 0.3) expressing FtsZ-mKate2 and incubated for 4 min at 37 °C before washing and fluorescence microscopy imaging. Phase contrast (grey) and fluorescent signals of mKate2 (red), GFP (green) and HADA images are shown. Scale bars: 1 µm. Cell division process is divided into i to v stages. (For interpretation of the references to colour in this figure caption, the reader is referred to the web version of this article.)

localization of sfGFPop-LytA is followed on a single cell throughout a complete cell cycle (Fig. 8 and Supplemental video S1). A comparable pattern was observed: in early division stage (Fig. 8 frame 4 min) sfGFPop-LytA localizes at the equator of the cell which is the site of the newly synthesized cell wall when cell undergoes division process (Fig. 8 frames 9–14 min) and remains associated to this position, which under the progress of the cell cycle gives rise to the cell poles (Fig. 8 frames 24 min to 64 min). Faint labeling at the new division site of daughter cells is also detected suggesting that sfGFPop-LytA from the initial labeled site can relocalize to the new cell wall synthesis sites (Fig. 8 frames 34 min and 44 min).

In conclusion, localization of sfGFPop-LytA at the division site follows the PG synthesis site as reported by HADA and remains associated to the cell poles. This observation is consistent with the timing of TAs insertion in the cell wall which persists at the division site after PG synthesis has ceased (Bonnet et al., submitted).

LytA binds to newly synthesized TAs

To investigate whether sfGFPop-LytA might recognize and bind to newly inserted TAs, TAs have been mapped on the surface of live pneumococcal cells. We have developed a method to metabolically label TAs by click chemistry. The choline-growth dependency of *S. pneumoniae* has been exploited to incorporate choline molecules bearing small functional groups ready for click chemistry when incorporated into the TAs polymers. Using Cu(I)-catalyzed azide-alkyne cycloaddition, fluorescent reporters were grafted to TAs decorated with the chemically modified choline molecules in a specific and selective manner (Di Guilmi et al., 2017). This method has been adapted to live cells using copper-free bioorthogonal click reaction and fluorescent reporter such as DIBO-Alexa Fluor 594 (Bonnet et al., submitted). Briefly, pneumococcal cells grown in the presence of normal choline were washed and incubated for 4 min with choline-N3, DIBO-Alexa594

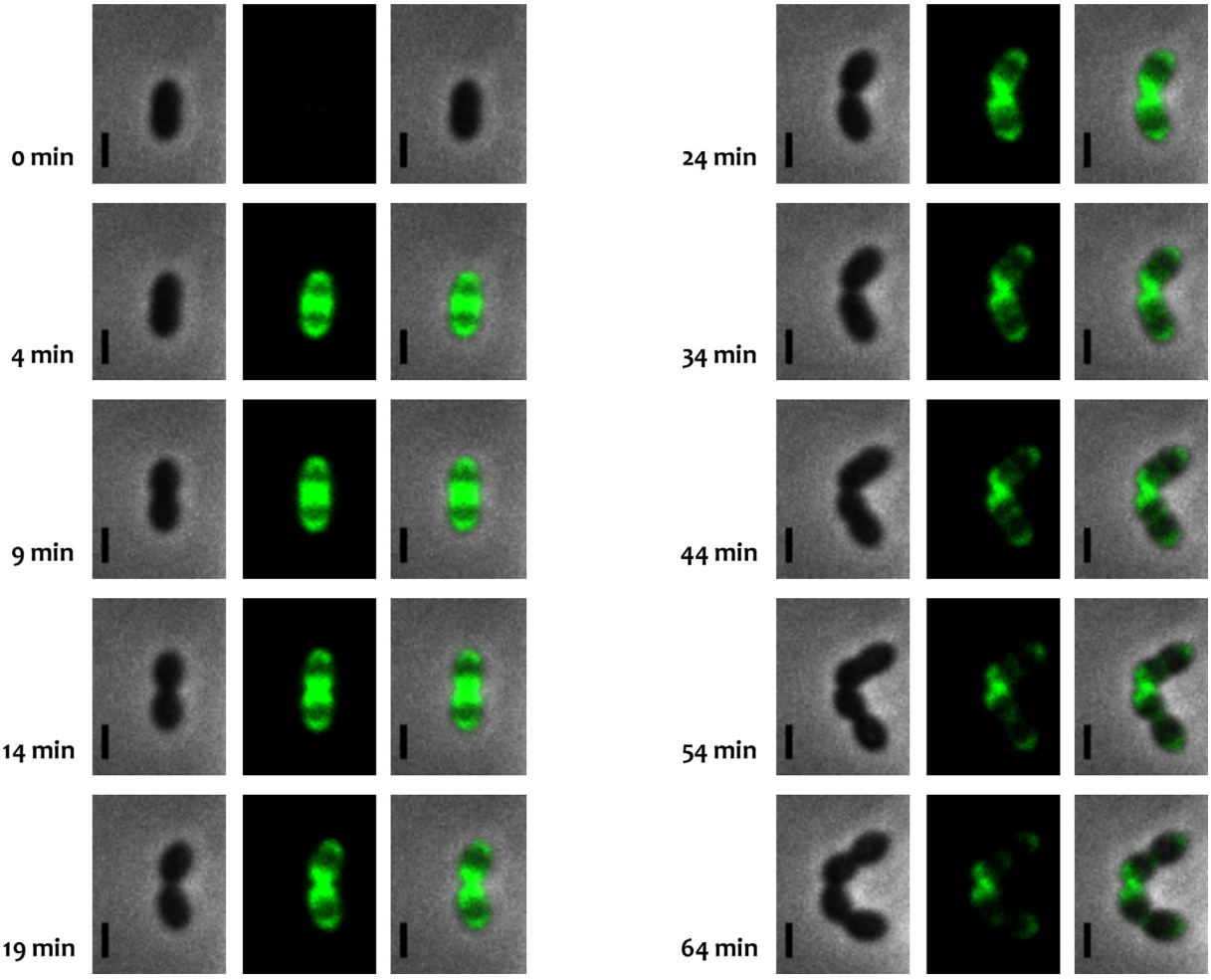

Fig. 8. Association of LytA to the nascent cell wall. Time-lapse images of WT cells labelled by sfGFPop-LytA (green) in a microfluidic system. sfGFPop-LytA was pulse-injected at 50 μg/ml on cells before extensive wash with CY medium (see Methods). The movie shows an overlay of GFP (green) and phase-contrast (grey) images. Scale bar: 1 μm. (For interpretation of the references to colour in this figure caption, the reader is referred to the web version of this article.)

and sfGFPop-LytA at 37 °C. After two washes, cell growth was pursued in C-medium supplemented with 4 μg/ml choline at 37 °C for different periods of time. Microscopy observations were performed immediately after the 4-min pulse period (0 min) and after a chase duration of 20 min and 40 min (Fig. 9). At t0, sfGFPop-LytA is perfectly co-localized with the newly cell wall-inserted and labeled TAs, positioned at the parental division site (yellow arrow) and daughter cells equators (cyan arrows). After a 20-min chase period, the cell wall-inserted and labeled TAs equators had split into two rings (viewed side-on) that move apart as PG synthesis elongates the cell while sfGFPop-LytA remained associated at mid-cell. After a 40-min chase period, once the cell division is complete, the cell wall-inserted and labeled TAs had moved to the newly equatorial sites. If cells have separated after their division, the TAs labeling is found on free hemispheres. Similar observations were achieved with sfGFPop-LytA^{CBD} (Fig. S5) showing that the dynamics of LytA localization is independent from the amidase activity. These data show that sfGFPop-LytA associates to newly cell wall-inserted TAs at the division site. Considering the dynamics of the cell wall synthesis, we hypothesize that sfGFPop-LytA binds to newly cell wall-inserted TAs and then dissociates from those TAs once they move apart due to cell wall elongation.

Discussion

A characteristic of the pneumococcal growth in laboratory culture condition is the occurrence of autolysis (Tomasz 1968), launched several hours after the beginning of the stationary phase and induced by the amidase LytA, which cleaves the amide bond between Mur*N*Ac and l-alanine (Howard and Gooder, 1974). Pneumococcal cells are protected from LytA lysis during the exponential growth phase but these protective features are lost upon entry into the stationary phase (Tomasz and Waks, 1975; Mellroth et al., 2012). Despite the long-standing identification of the role of LytA as the major pneumococcal autolysin, the molecular mechanisms of its regulation are still poorly understood.

In this work, we show by two complementary approaches that the sensitivity of growing pneumococcal cells to LytA is challenged by the level of TAs present at the cell surface. Firstly, the modulation of the concentration of choline into the culture medium impacts the activity of LytA since depletion of choline increases the sensitivity of cells to LytA-induced lysis. One would expect that in conditions where TAs would be poorly decorated by choline (when choline is supplemented at low concentration), less LytA molecules would bind, thereby reducing the LytA-induced lysis. However, our data show the opposite effect indicating that the hydrolase activity of LytA is not directly correlated to the quantity of protein bound at the cell surface. It has been proposed that the flippase TacF would specifically transports TAs loaded in choline across the membrane (Damjanovic et al., 2007; González et al., 2008; Kharat et al., 2008; Denapaite et al., 2012 for review). Consequently, the choline depletion could negatively impact TAs synthesis and/or TAs translocation across the membrane. Secondly, we generated viable pneumococcal strain depleted in *tarI* and *tarJ* genes which should

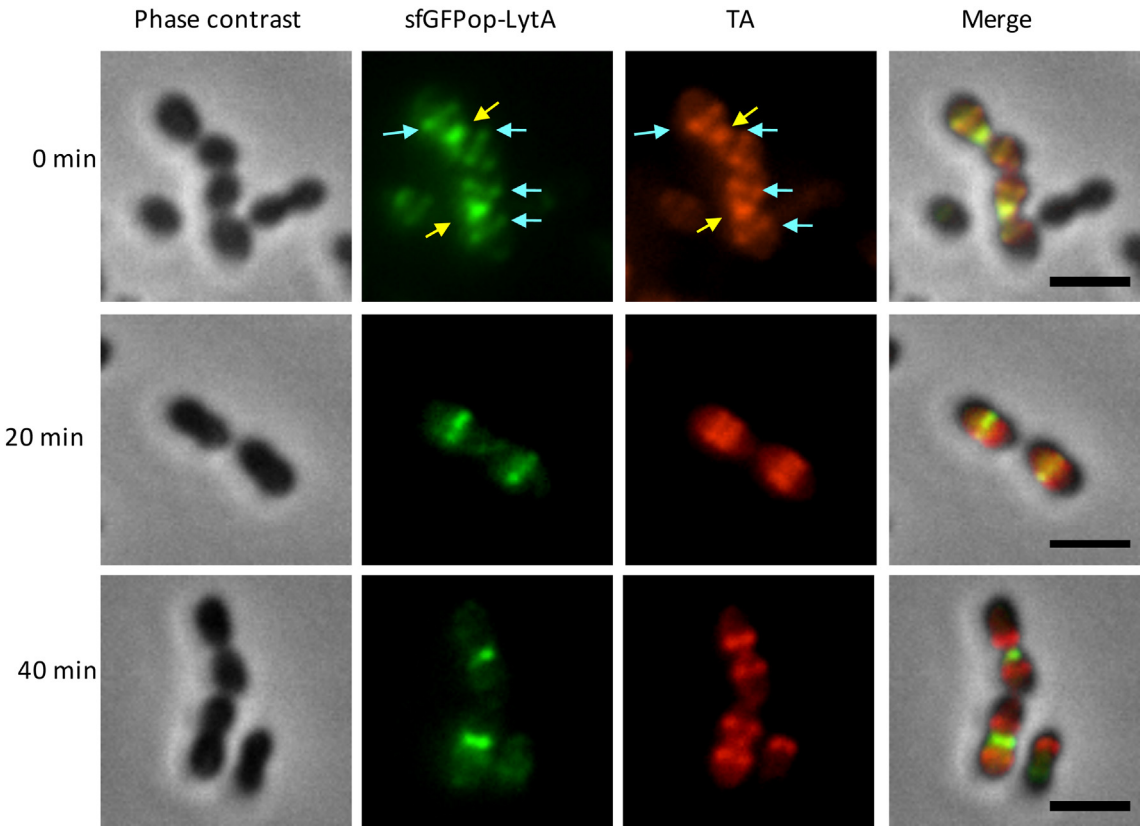

Fig. 9. LytA binds to newly synthesized TAs positioned at the septal cross-wall site. Pneumococcal cells grown in the presence of normal choline were washed at $OD_{600\,nm}$ 0.3 and incubated for 4 min with choline-N3, DIBO and sfGFPop-LytA. After two washes, cell growth was pursued in CY at 37 °C. Microscopy observations were performed immediately after the 4-min pulse period (0 min) and after a chase duration of 20 min and 40 min. Phase contrast (grey), fluorescent signals of TAs labelled with DIBO-Alexa594 (red), GFP (green) and merge images are shown. The parental cross-wall septal site is indicated by yellow arrows and the daughter new septal site by cyan arrows. Scale bars: 2 µm. (For interpretation of the references to colour in this figure caption, the reader is referred to the web version of this article.)

produce reduced amount of TAs. This strain also displays an increased sensitivity towards LytA in a comparable manner to the condition of choline starvation. These results indicate that when the amount of TAs is strongly reduced in the cell wall, the structure of PG might be modified to favor the access of LytA to the targeted Mur*N*Ac – l-alanine amide bond. We described a similar effect when Mur*N*Ac residues are not O-acetylated (Bonnet et al., 2017). Altogether, these data suggest that the structuration of the PG network can be regulated, for example by Mur*N*Ac O-acetylation and/or by the proximity of TAs.

The *tarIJ* pneumococcal mutant strain displays shape defects confirming the roles of TAs in cell morphology and cell division. Indeed, Gram-positive bacteria that display reduced amounts of TAs (through inactivation of WTAs or LTAs encoding genes) present abnormal cell shapes and sizes, irregular cell wall thickness and abnormal septa positioning, strongly supporting a tight coordination between PG and TAs biosynthesis to build the cell wall. In addition, the failure of mutants to efficiently divide and separate during cell division implicates a role of TAs in coordinating the localization, stability, and/or activity of PG hydrolases. Inactivation of genes encoding WTAs or LTAs was achieved in *B. subtilis* and *S. aureus* by disrupting the first-acting genes involved in the respective biosynthetic pathways, while the combination of the two deletions appeared to be lethal, indicating that TAs are essential for the formation of the cell wall and/or for cell survival (D'Elia et al., 2006a,b; Grundling and Schneewind, 2007; Schirner et al., 2009; Oku et al., 2009). *B. subtilis* WTAs mutants appear affected in cell elongation (D'Elia et al., 2006b) while septation and cell division are abnormal in LTAs mutants (Schirner et al., 2009) suggesting that WTAs and LTAs would be specialized for elongation and division processes, respectively. These observations seem to be restricted to bacilli species since *S. aureus* blocked in WTAs synthesis have extensive defects in septation and cell separation (Campbell et al., 2011). Further evidences suggesting that TAs synthesis is coupled to cell division come from the observation that the localization of proteins involved in the WTAs and LTAs synthesis in *B. subtilis* displayed a pattern similar to that of nascent PG at the division site (Formstone et al., 2008; Schirner et al., 2009).

A functional link between TAs and PG hydrolases during cell division has been reported in *B. subtilis* and *S. aureus* (Yamamoto et al., 2008; Kiriyama et al., 2014; Schlag et al., 2010). Cell separation in *B. subtilis* depends on the cleavage of PG by DL-endopeptidases among which LytF plays an active role. It has been shown that LytF binding to PG as well as its sidewall subcellular localization are inhibited both by WTAs (Yamamoto et al., 2008) and a comparable effect by LTAs has also been described (Kiriyama et al., 2014). The staphylococcal bifunctional autolysin Atl is localized at the septal region where it exerts its PG hydrolytic activities to efficiently allow cell separation. The positioning of Atl is regulated by WTAs: by preventing binding of Atl to the old cell wall but not to the cross-wall site, WTAs favors the separation of daughter cells (Schlag et al., 2010). Lastly, WTAs by contributing to the proton-binding capacity of *S. aureus* cell walls, influence the autolysis rate via the major autolysin Atl (Biswas et al., 2012). The sum of these data indicates that TAs control PG remodeling, and therefore impact cell morphogenesis, by directing the subcellular localization of key PG hydrolytic enzymes. Whether i) PG hydrolases directly bind to TAs and ii) TAs guide the enzymes to the right place at the right time during the cell cycle is still unclear.

We addressed these questions by investigating the localization of the LytA-sfGFPop form expressed in the pneumococcal cells and observed that it varies according to growth-phase. LytA was diffuse into

the cytoplasm during the exponential phase. During the progression to stationary phase, the fluorescence was reorganized into micro-domains, either associated to the inner face of the cytoplasmic membrane or randomly distributed into the cytoplasm. When released during the lytic phase, LytA-sfGFPop binds at the surface of non-lyzed neighbouring cells at mid-cell position. Our data regarding LytA subcellular distribution confirmed the data previously published (Mellroth et al., 2012). Indeed, lytA starts to be released at the end of the exponential phase and growing amount of the protein is present in the medium and associates to neighboring cells until a threshold is reached during stationary phase leading to the lysis of the entire population. The inactive form of LytA displayed a localization pattern and an association level at the cell surface comparable to the LytA active form, indicating that the release of LytA does not depend on its amidase activity. However, both the amidase and CBD domains are required to exert the lytic activity, including the release from the cytoplasm and the binding to TAs.

We exploited the characteristic of the CBPs to bind to choline-associated TAs when added exogenously to pneumococcal cells. The binding pattern of LytA fused to sfGFPop was followed in diverse conditions. First, the full-length LytA and the isolated CBD proteins were compared. Similar behaviors were observed, indicating that the localization of LytA at the cell surface is triggered by the association to TAs through the CBD. We observed that LytA is present in the hot spot of active cross-wall synthesis. Since LytA is specifically associated to TAs, we propose that LytA binds to newly synthesized TAs incorporated into the nascent cross-wall. In support of this idea, our pulse-chase experiments reveal that the synthesis of TAs occurs at the division site, confirming pioneering work performed by Briles and Tomasz in 1970. Co-localization data show that LytA binds to TAs inserted at the division site where PG cross-wall is also formed. Although TAs are present all over the cell surface (Briles and Tomasz, 1970; Bonnet et al., submitted), no association of LytA to TAs present in the peripheral cell wall has been observed. This observation suggests that (i) different TAs species are present in the septal and the peripheral walls, (ii) septal TAs might be submitted to a modification/maturation process very soon after its synthesis (or translocation), hence impeding LytA recognition and binding. The molecular determinants that make neo-synthesized TAs specifically recognized by LytA remain to be deciphered. Whether this population is enriched in LTAs or WTAs or display particular degree of choline decoration are some of the many important questions to be addressed in the near future.

Conflicts of interest

The authors declare no conflicts of interest.

Acknowledgements

This work used the platforms of the Grenoble Instruct-ERIC centre (ISBG; UMS 3518 CNRS-CEA-UGA-EMBL) with support from FRISBI (ANR-10-INSB-05-02) and GRAL (ANRS-10-LABX-49-01) within the Grenoble Partnership for Structural Biology (PSB). The electron microscopy facility is supported by the Rhône-Alpes Region, the Fondation pour la Recherche Médicale (FRM), the fonds FEDER, and the GIS-Infrastructures en Biologie Santé et Agronomie (IBISA). J.B. received a PhD fellowship from the French Ministry of Education and Research. We thank Kousik Sundararajan for assistance with TEM (Hilde Kolstad, Norway) Yves Brun, Erkin Kuru and Michael van Nieuwenzhe (Bloomington University) for providing HADA and Guy Schoehn for support. We are grateful to André Zapun for helpful discussions.

Appendix A. Supplementary data

Supplementary data associated with this article can be found, in the online version, at http://dx.doi.org/10.1016/j.tcsw.2018.05.001.

References

Baur, S., Marles-Wright, J., Buckenmaier, S., Lewis, R.J., Voller, W., 2009. Synthesis of CDP-activated ribitol for teichoic acid precursors in *Streptococcus pneumoniae*. J. Bacteriol. 191, 1200–1210.

Berg, K.H., Biørnstad, T.J., Straume, D., Håvarstein, L.S., 2011. Peptide-regulated gene depletion system developed for use in *Streptococcus pneumoniae*. J. Bacteriol. 193, 5207–5215.

Berg, K.H., Stamsås, G.A., Straume, D., Håvarstein, L.S., 2013. Effects of low PBP2b levels on cell morphology and peptidoglycan composition in *Streptococcus pneumoniae* R6. J. Bacteriol. 195, 4342–4354.

Biswas, R., Martinez, R.E., Göhring, N., Schlag, M., Josten, M., Xia, G., et al., 2012. Proton-binding capacity of *Staphylococcus aureus* Wall Teichoic Acid and its role in controlling autolysin activity. PLoS One 7, e41415.

Bonnet, J., Durmort, C., Jacq, M., Mortier-Barrière, I., Campo, N., VanNieuwenhze, M.S., Brun, Y.V., Arthaud, C., Gallet, B., Moriscot, C., Morlot, C., Vernet, T., Di Guilmi, A.M., 2017. Peptidoglycan O-acetylation is functionally related to cell wall biosynthesis and cell division in *Streptococcus pneumoniae*. Mol. Microbiol. 106, 832–846.

Briles, E.B., Tomasz, A., 1970. Radioautographic evidence for equatorial wall growth in a Gram-positive bacterium. Segregation of choline-^{3}H-labeled teichoic acid. J. Cell. Biol. 47, 786–790.

Brown, S., Santa Maria Jr., J.P., Walker, S., 2013. Wall teichoic acids of Gram-positive bacteria. Annu. Rev. Microbiol. 67, 313–336.

Bryant, J.C., Dabbs, R.C., Oswalt, K.L., Brown, L.R., Rosch, J.W., Seo, K.S., Donaldson, J.R., McDaniel, L.S., Thornton, J.A., 2016. Pyruvate oxidase of *Streptococcus pneumoniae* contributes to pneumolysin release. BMC Microbiol. 16, 271.

Campbell, J., Singh, A.K., Santa Maria Jr., J.P., Kim, Y., Brown, S., Swoboda, J.G., Mylonakis, E., Wilkinson, B.J., Walker, S., 2011. Synthetic lethal compound combinations reveal a fundamental connection between wall teichoic acid and peptidoglycan biosyntheses in *Staphylococcus aureus*. ACS Chem. Biol. 6, 106–116.

Damjanovic, M., Kharat, A.S., Eberhardt, A., Tomasz, A., Vollmer, W., 2007. The essential tacF gene is responsible for the choline-dependent growth phenotype of *Streptococcus pneumoniae*. J. Bacteriol. 189, 7105–7111.

D'Elia, M.A., Pereira, M.P., Chung, Y.S., Zhao, W., Chau, A., Kenney, T.J., Sulavik, M.C., Black, T.A., Brown, E.D., 2006a. Lesions in teichoic acid biosynthesis in *Staphylococcus aureus* lead to a lethal gain of function in the otherwise dispensable pathway. J. Bacteriol. 188, 4183–4189.

D'Elia, M.A., Millar, K.E., Beveridge, T.J., Brown, E.D., 2006b. Wall teichoic acid polymers are dispensable for cell viability in *Bacillus subtilis*. J. Bacteriol. 188, 8313–8316.

Denapaite, D., Brückner, R., Hakenbeck, R., Vollmer, W., 2012. Biosynthesis of teichoic acids in *Streptococcus pneumoniae* and closely related species: lessons from genomes. Microbial Drug Resistance 18, 344–358.

Di Guilmi, A.M., Bonnet, J., Peiβert, S., Durmort, C., Gallet, B., Vernet, T., Gisch, N., Wong, Y.S., 2017. Specific and spatial labeling of choline-containing teichoic acids in *Streptococcus pneumoniae* by click chemistry. Chem. Commun. (Camb). 53, 10572–10575.

Eberhardt, A., Wu, L.J., Errington, J., Vollmer, W., Veening, J.W., 2009. Cellular localization of choline-utilization proteins in *Streptococcus pneumoniae* using novel fluorescent reporter systems. Mol. Microbiol. 74, 395–408.

Egan, A.J.F., Biboy, J., van't Veer, I., Breukink, E., Vollmer, W., 2015. Activities and regulation of peptidoglycan synthases. Phil. Trans. R. Soc. B 370, 20150031.

Eldholm, V., Johnsborg, O., Haugen, K., Ohnstad, H.S., Håvarstein, L.S., 2009. Fratricide in *Streptococcus pneumoniae*: Contributions and role of the cell wall hydrolases CbpD, LytA and LytC. Microbiology 155, 2223–2234.

Emami, K., Guyet, A., Kawai, Y., Devi, J., Wu, L.J., Allenby, N., et al., 2017. RodA as the missing glycosyltransferase in *Bacillus subtilis* and antibiotic discovery for the peptidoglycan polymerase pathway. Nat. Microbiol. 2, 16253.

Formstone, A., Carballido-Lopez, R., Noirot, P., Errington, J., Scheffers, D.J., 2008. Localization and interactions of teichoic acid synthetic enzymes in *Bacillus subtilis*. J. Bacteriol. 190, 1812–1821.

Frolet, C., Beniazza, M., Roux, L., Gallet, B., Noirclerc-Savoye, M., Vernet, T., Di Guilmi, A.M., 2010. New adhesin functions of surface-exposed pneumococcal proteins. BMC Microbiology 10, 190.

Johnsborg, O., Eldholm, V., Bjørnstad, M.L., Håvarstein, L.S., 2008. A predatory mechanism dramatically increases the efficiency of lateral gene transfer in *Streptococcus pneumoniae* and related commensal species. Mol. Microbiol. 69, 245–253.

Johnsborg, O., Håvarstein, L.S., 2009. Pneumococcal LytR, a protein from the LytR-CpsA-Psr family, is essential for normal septum formation in *Streptococcus pneumoniae*. J. Bacteriol. 191, 5859–5864.

González, A., Llull, D., Morales, M., García, P., García, E., 2008. Mutations in the *tacF* gene of clinical strains and laboratory transformants of *Streptococcus pneumoniae*: impact on choline auxotrophy and growth rate. J. Bacteriol. 190, 4129–4138.

Grundling, A., Schneewind, O., 2007. Synthesis of glycerol phosphate lipoteichoic acid in *Staphylococcus aureus*. Proc. Natl. Acad. Sci. U.S.A. 104, 8478–8483.

Higuchi, R., Krummel, B., Saiki, R.K., 1988. A general method of in vitro preparation and specific mutagenesis of DNA fragments: study of protein and DNA interactions. Nucl. Acids Res. 16, 7351–7367.

Howard, L.V., Gooder, H., 1974. Specificity of the autolysin of *Streptococcus (Diplococcus) pneumoniae*. J. Bacteriol. 117, 796–804.

Hugonnet, J.E., Mengin-Lecreulx, D., Monton, A., den Blaauwen, T., Carbonnelle, E., Veckerlé, C., Brun, Y.V., van Nieuwenhze, M., Bouchier, C., Tu, K., Rice, L.B., Arthur, M., 2016. Factors essential for L,D-transpeptidase-mediated peptidoglycan cross-linking and β-lactam resistance in Escherichia coli. Elife e19469. doi:10.7554/eLife.19469.

Kharat, A.S., Denapaite, D., Gehre, F., Brückner, R., Vollmer, W., Hakenbeck, R., Tomasz, A., 2008. Different pathways of choline metabolism in two choline-independent strains of Streptococcus pneumoniae and their impact on virulence. J. Bacteriol. 190, 5907–5914.

Kiriyama, Y., Yazawa, K., Tanaka, T., Yoshikawa, R., Yamane, H., Hashimoto, M., Sekiguchi, J., Yamamoto, H., 2014. Localization and expression of the *Bacillus subtilis* DL-endopeptidase LytF are influenced by mutations in LTA synthases and glycolipid anchor synthetic enzymes. Microbiology 160, 2639–2649.

Kuru, E., Velocity Hughes, H., Brown, P.J., Hall, E., Tekkam, S., Cava, F., et al., 2012. In situ probing of newly synthesized peptidoglycan in live bacteria with fluorescent D-amino acids. Angew. Chem. Int. Ed. Engl. 51, 12519–12523.

Lacks, S., Hotchkiss, K.D., 1960. A study of the genetic material determining an enzyme in *Pneumococcus*. Biochim. Biophy. Acta 39, 508–518.

McPherson, D.C., Popham, D.L., 2003. Peptidoglycan synthesis in the absence of class A penicillin-binding proteins in *Bacillus subtilis*. J. Bacteriol. 185, 1423–1431.

Mellroth, P., Daniels, R., Eberhardt, A., Rönnlund, D., Blom, H., Widengren, J., et al., 2012. LytA, major autolysin of *Streptococcus pneumoniae*, requires access to nascent peptidoglycan. J. Biol. Chem. 287, 11018–11029.

Morlot, C., Bayle, L., Jacq, M., Fleurie, A., Tourcier, G., Galisson, F., et al., 2013. Interaction of Penicillin-Binding Protein 2x and Ser/Thr protein kinase StkP, two key players in *Streptococcus pneumoniae* R6 morphogenesis. Mol. Microbiol. 90, 88–102.

Oku, Y., Kurokawa, K., Matsuo, M., Yamada, S., Lee, B.L., Sekimizu, K., 2009. Pleiotropic roles of polyglycerolphosphate synthase of lipoteichoic acid in growth of *Staphylococcus aureus* cells. J. Bacteriol. 191, 141–151.

Paintdakhi, A., Parry, B., Campos, M., Irnov, I., Elf, J., Surovtsev, I., et al., 2016. Oufti: an integrated software package for high-accuracy, high-throughput quantitative microscopy analysis. Mol. Microbiol. 99, 767–777.

Pagliero, E., Dublet, B., Frehel, C., Dideberg, O., Vernet, T., Di Guilmi, A.M., 2008. The inactivation of a new peptidoglycan hydrolase Pmp23 leads to abnormal septum formation in *Streptococcus pneumoniae*. The Open Microbiol. J. 2, 107–114.

Pédelacq, J.D., Cabantous, S., Tran, T., Terwilliger, T.C., Waldo, G.S., 2006. Engineering and characterization of a superfolder green fluorescent protein. Nat. Biotechnol. 24, 79–88.

Percy, M.G., Gründling, A., 2014. Lipoteichoic acid synthesis and function in Gram-positive bacteria. Annu. Rev. Microbiol. 68, 81–100.

Philippe, J., Gallet, B., Morlot, C., Denapaite, D., Hakenbeck, R., Chen, Y., et al., 2015. Mechanism of β-lactam action in *Streptococcus pneumoniae*: the piperacillin paradox. Antimicrob. Agents Chemother. 59, 609–621.

Regev-Yochay, G., Trzcinski, K., Thompson, C.M., Lipsitch, M., Malley, R., 2007. SpxB is a suicide gene of *Streptococcus pneumoniae* and confers a selective advantage in an *in vivo* competitive colonization model. J. Bacteriol. 189, 6532–6539.

Sauvage, E., Terrak, M., 2016. Glycosyltransferases and Transpeptidases/Penicillin-Binding Proteins: valuable targets for new antibacterials. Antibiotics 5, 12.

Schirner, K., Marles-Wright, J., Lewis, R.J., Errington, J., 2009. Distinct and essential morphogenic functions for wall- and lipoteichoic acids in *Bacillus subtilis*. EMBO J. 28, 830–842.

Schlag, M., Biswas, R., Krismer, B., Kohler, T., Zoll, S., Yu, W., Schwarz, H., Peschel, A., Götz, F., 2010. Role of staphylococcal wall teichoic acid in targeting the major autolysin Atl. Mol. Microbiol. 75, 864–873.

Sliusarenko, O., Heinritz, J., Emonet, T., Jacobs-Wagner, C., 2011. High-throughput, subpixel precision analysis of bacterial morphogenesis and intracellular spatio-temporal dynamics. Mol. Microbiol. 80, 612–627.

Straume, D., Stamsås, G.A., Salehian, Z., Håvarstein, L.S., 2017. Overexpression of the fratricide immunity protein ComM leads to growth inhibition and morphological abnormalities in *Streptococcus pneumoniae*. Microbiology 163, 9–21.

Sung, C.K., Li, H., Claverys, J.P., Morrison, D.A., 2001. An *rpsL* cassette, *Janus*, for gene replacement through negative selection in *Streptococcus pneumoniae*. Appl. Environ. Microbiol. 67, 5190–5196.

Tomasz, A., 1968. Biological consequences of the replacement of choline by ethanolamine in the cell wall of pneumococcus: chain formation, loss of transformability, and loss of autolysis. Proc. Natl. Acad. Sci. U.S.A. 59, 86–93.

Tomasz, A., Waks, S., 1975. Mechanism of action of penicillin: triggering of the pneumococcal autolytic enzyme by inhibitors of cell wall synthesis. Proc. Natl. Acad. Sci. U.S.A. 72, 4162–4166.

Vollmer, W., Joris, B., Charlier, P., Foster, S., 2008. Bacterial peptidoglycan (murein) hydrolases. FEMS Microbiol. Rev. 32, 259–286.

Yamamoto, H., Miyake, Y., Hisaoka, M., Kurosawa, S., Sekiguchi, J., 2008. The major and minor wall teichoic acids prevent the sidewall localization of vegetative dl-endopeptidase LytF in *Bacillus subtilis*. Mol. Microbiol. 70, 297–310.

Yother, J., White, J.M., 1994. Novel surface attachment mechanism of the *Streptococcus pneumoniae* protein PspA. J. Bacteriol. 176, 2976–2985.